Publication Year	2017
Acceptance in OA	2020-09-18T13:18:23Z
Title	False outliers of the Ep,i – Eiso correlation?
Authors	Martone, R., Izzo, L., DELLA VALLE, Massimo, AMATI, LORENZO, Longo, G., Götz, D.
Publisher's version (DOI)	10.1051/0004-6361/201730704
Handle	http://hdl.handle.net/20.500.12386/27449
Journal	ASTRONOMY & ASTROPHYSICS
Volume	608

A&A 608, A52 (2017)
DOI: 10.1051/0004-6361/201730704
© ESO 2017

Astronomy & Astrophysics

False outliers of the $E_{p,i} - E_{iso}$ correlation?

R. Martone[1,2], L. Izzo[3], M. Della Valle[4,5], L. Amati[6], G. Longo[2], and D. Götz[7]

[1] Dipartimento di Fisica e Scienze della Terra, Universitá di Ferrara, via Saragat 1, 44122 Ferrara, Italy
e-mail: mrtrnt@unife.it
[2] Universitá di Napoli "Federico II", Dipartimento di Fisica "Ettore Pancini", C. U. Monte S. Angelo, 80126 Napoli, Italy
[3] Instituto de Astrofisica de Andalucia (IAA-CSIC), Glorieta de la Astronomia s/n, 18008 Granada, Spain
[4] INAF–Osservatorio Astronomico di Napoli, Salita Moiariello, 16, 80131 Napoli, Italy
[5] International Center for Relativistic Astrophysics, Piazza della Repubblica 10, 65122 Pescara, Italy
[6] INAF–IASF Bologna, via P. Gobetti, 101, 40129 Bologna, Italy
[7] AIM–CEA/DRF/Irfu/Service d'Astrophysique, Orme des Merisiers, 91191 Gif-sur-Yvette, France

Received 27 February 2017 / Accepted 9 August 2017

ABSTRACT

Context. In the context of an in-depth understanding of GRBs and their possible use in cosmology, some important correlations between the parameters that describe their emission have been discovered, among which the "$E_{p,i} - E_{iso}$" correlation is the most studied. Because of this, it is fundamental to shed light on the peculiar behaviour of a few events, namely GRB 980425 and GRB 031203, that appear to be important outliers of the $E_{p,i} - E_{iso}$ correlation.
Aims. In this paper we investigate if the locations of GRB 980425 and GRB 031203, the two (apparent) outliers of the correlation, may be due to an observational bias caused by the lacking detection of the soft X-ray emissions associated with these GRBs, from respectively the Burst And Transient Source Experiment (BATSE) detector on-board the Compton Gamma-Ray Observer and INTEGRAL, that were operating at the epoch at which the observations were carried out. We analyse the observed emission of other similar sub-energetic bursts (GRBs 060218, 100316D and 161219B) observed by *Swift* and whose integrated emissions match the $E_{p,i} - E_{iso}$ relation. We simulate their integrated and time-resolved emissions as would have been observed by the same detectors that observed GRB 980425 and GRB 031203, aimed at reconstructing the light curve and spectra of these bursts.
Methods. We estimate the $E_{p,i}$ and the E_{iso} parameters from the time-resolved and total integrated simulated spectra of GRBs 060218, 100316D and 161219B as observed by *Beppo*SAX, BATSE, INTEGRAL, and the Wide Field Monitor (WFM) proposed for the Large Observatory For X-ray Timing (LOFT) and enhanced X-ray Timing and Polarimetry (eXTP) missions.
Results. If observed by old generation instruments, GRBs 060218, 100316D, and 161219B would appear as outliers of the $E_{p,i}$–E_{iso} relation, while if observed with *Swift* or the WFM GRB 060218 would perfectly match the correlation. We also note that the instrument BAT alone (15−150 keV) did measure GRB 060218 as an outlier.
Conclusions. We suggest that if GRB 980425 and GRB 031203 would have been observed by *Swift* and by eXTP, they might have matched the $E_{p,i}$–E_{iso} relation. This provides strong support to the idea that instrumental biases can cause some events in the lower left corner of the $E_{p,i} - E_{iso}$ plane to appear as outliers of the so-called Amati relation.

Key words. gamma-ray burst: general – gamma-ray burst: individual: GRB 060218 – methods: data analysis

1. Introduction

Observations of long-duration gamma-ray bursts (GRBs) in the past decades have shown the many empirical relations that link some of the fundamental parameters of GRBs such, as the isotropic energy E_{iso} that is emitted in gamma rays, and the peak energy of the prompt emission spectrum $E_{p,i}$, the peak luminosity L_p of the prompt emission (Amati et al. 2002; Ghirlanda et al. 2004; Yonetoku et al. 2004; Liang & Zhang 2005; Dainotti et al. 2008; Bernardini et al. 2012; Margutti et al. 2013; Izzo et al. 2015).

We focus on the most popular of them, the $E_{p,i} - E_{iso}$ correlation, which is also known as the Amati relation (Amati et al. 2002; Amati 2006). This relation stated that the total gamma-ray isotropic energy (E_{iso}) emitted in long GRBs correlates with the rest-frame value of the energy spectrum at which their gamma-ray emission peak ($E_{p,i}$). We here estimate the isotropic output using the quantity $E_{\gamma,iso}$, which represents the total energetic output in the rest-frame range 1−10 000 keV.

To date more than 200 GRBs match the $E_{p,i}$–E_{iso} relation; however, after 20 yr, it is still debated that the closest GRBs ever discovered, GRB 980425 at $z = 0.0085$ ($d = 40$ Mpc), appears to be a remarkable outlier of the Amati relation (Ghisellini et al. 2006; Amati 2006). This situation is still more disturbing after noting that GRB 980425 was found to be the first GRB associated with a supernova (SN), the SN 1998bw (Galama et al. 1998), and therefore it is recognized as the prototype of the GRB-SN connection (Woosley & Bloom 2006; Della Valle 2011). The existence of outliers of the Amati relation should also be clarified in view of both understanding the emission processes at play in the GRB phenomenon and the frequent use of GRBs in cosmological studies (Amati et al. 2008; Amati & Della Valle 2013; Izzo et al. 2015). We suggest that the location of GRB 980425 in the $E_{p,i} - E_{iso}$ plane is very likely due to an observational bias caused by the sensitivity range 25−2000 keV of the Burst And Transient Source Experiment (BATSE) detector on board the Compton Gamma-Ray Observer (CGRO; Meegan et al. 1992). Similar arguments apply to the case of an other sub-energetic and nearby ($z = 0.105$) event: GRB 031203 (Mazzali et al. 2006; Watson et al. 2006).

To reach our goal, we show that nearby and sub-energetic bursts with an associated SN, GRB 060218 (Campana et al. 2006), GRB 100316D (Starling et al. 2011) and GRB 161219B (Cano et al. 2017) observed by the *Swift* Burst Alert Telescope

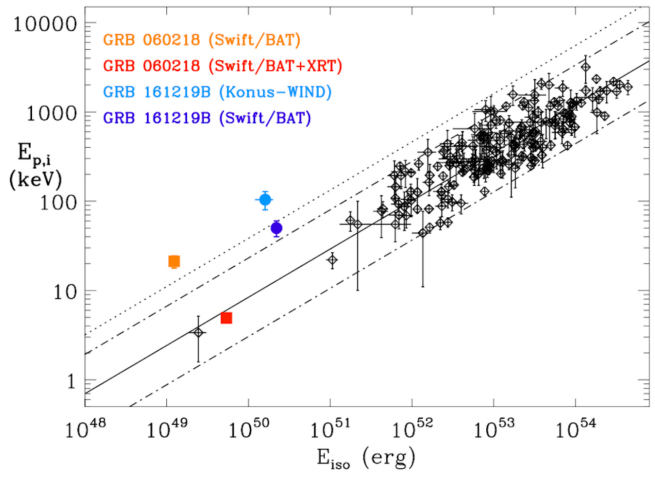

Fig. 1. Location in the $E_{p,i}$ – E_{iso} plane of GRB 161219B as observed by *Swift*-BAT and Konus-WIND and of GRB 060218 as observed by *Swift*-BAT and by *Swift*-BAT+XRT. *Swift*-BAT is more sensitive than Konus-WIND, thus allowing a more precise estimate of the $E_{p,i}$ and E_{iso} parameters for GRB 161219B and finding it more consistent with the Amati relation. In the outstanding case of GRB 060218, the emission in the soft X-ray band, which can only be detected by using *Swift*-XRT, makes this event, which otherwise would have been classified as an outlier, fully consistent with the $E_{p,i}$ – E_{iso} correlation. In the plot, the dot-dashed (dotted) lines refer to the 2 (3) sigma error around the best-fit line.

(BAT; Barthelmy et al. 2005) in the energy range 15−150 keV and the X-Ray Telescope (XRT; Burrows et al. 2005) in the energy range 0.3−10 keV, consistent with the $E_{p,i}$ – E_{iso} relation, would appear as outliers of the Amati relation if they had been observed with BATSE.

These GRBs are perfect for our purposes because, unlike other similar low-energetic events, they have a continuous coverage in time of their prompt emission by *Swift*-BAT, and in the case of GRB 060218 and GRB 100316D, also by XRT. The importance of the different instrument characteristics in determining the position of an event in the $E_{p,i}$ – E_{iso} plane can be appreciated considering Fig. 1, where we highlight the positions of GRB 060218 and GRB 161219B according to different detectors: it is clearly visible that when using measurements by instruments with better sensitivity and lower energy threshold these events become more consistent with the correlation. GRB 060218 is the emblem of this kind of behaviour, perfectly matching the best-fit of the $E_{p,i}$ – E_{iso} correlation when seen by *Swift*-XRT+BAT, and appearing as an outlier when observed with *Swift*-BAT alone, as we show in this work.

This work is organized as follows: in Sect. 2 we present the spectral properties of GRBs 060218, 100316D and 161219B and we introduce the method at the base of this paper. In Sect. 3 we describe the spectral analysis of these three GRBs, and in Sect. 4 we present the simulations of these GRBs as if they were observed by BATSE and other detectors. In the last section we report our conclusions.

2. *Swift* data analysis

In the following part of this article, we mainly focus on the case of GRB 060218, which presents one of the best datasets of the observed GRBs. Additional material regarding GRB 100316D and GRB 161219B, such as figures and tables, can be found in the appendix.

2.1. GRB 060218

GRB 060218 was discovered by *Swift* (Campana et al. 2006) and was found to be associated with SN 2006aj (Pian et al. 2006) at the redshift of $z = 0.0331$. Soft X-ray observations pointed out the presence of a thermal component, which originated in the breakout of a shock propagating into the wind surrounding the progenitor star (Campana et al. 2006; Waxman et al. 2007). The main feature that distinguish this GRB from more energetic GRBs is the long duration (∼3000 s) of the prompt emission observed down to X-rays, which is clearly different from the canonical emission observed in almost all GRBs (Nousek et al. 2006). Thanks to this very long duration (and its proximity) it was possible to detect most of the prompt emission with both BAT (15−150 keV) and XRT (0.2−10 keV). The integrated BAT+XRT spectrum is characterized by an intrinsic peak energy of $E_{p,i} = 4.9$ keV and a total integrated isotropic energy of $E_{iso} = 6.2 \times 10^{49}$ erg. With these values, GRB 060218 matches the Amati relation (see Fig. 6).

Owing to its low luminosity, low redshift, and the associated Sn, GRB 060218 has been considered a "twin" of GRB 980425 and GRB 031203 (Ghisellini et al. 2006), but it shows a different time duration and high-energy emission. It is consequently very interesting to derive the spectrum of GRB 060218 and its location in the $E_{p,i}$ – E_{iso} plane as it would have been observed by the same instruments as observed GRB 980425 (*Beppo*SAX, Frontera et al. 2000; BATSE, Meegan et al. 1992) and GRB 031203 (INTEGRAL, Mereghetti et al. 2003). We also consider the case for eXTP (Amati et al. 2013; Zhang et al. 2016), a planned mission dedicated to observing the X-ray transient sky in the soft X-ray energies.

We have reproduced the *Swift* data analysis as reported in Campana et al. (2006) using the same time intervals, and the results are reported in Fig. 2. The XRT spectral data were obtained for the corresponding BAT time intervals following the canonical procedure for GRB data reduction, starting with the `xrtpipeline` package, which runs all the tasks for XRT data processing in sequence. Since the X-ray emission from GRB 060218 was very bright, we applied the pile-up correction for the Window Timing mode, as the source presented count rates higher than 100 counts s^{-1} for a large part of its emission. We therefore selected a box with an annulus centred on the brightest pixel, as has been well described in Romano et al. (2006). After the pile-up correction, we obtained background files with XSELECT and generated the corresponding ancillary response function file with the `xrtmkarf` package. Finally, we grouped the data in order to have at least ten counts in each spectral bin; for this, we used the `grppha` package.

Since the complete dataset is composed of four spectra for which there are no XRT data, we divided the sample into two sub-datasets: 1) the first 4 BAT spectra lasting a total of $t_{D1} = 340$ s, and 2) the following 12 BAT and XRT spectra, lasting a total of $t_{D2} = 2387$ s and which cover the range 0.3–150 keV, with a data gap between 10–15 keV. The spectral data analysis was performed using the XSPEC fitting package (Arnaud 1996), assuming solar abundances as given in Wilms et al. (2000) and a cosmological model with $\Omega_\Lambda = 0.73$, $H_0 = 70\,\mathrm{km\,s^{-1}\,Mpc^{-1}}$ and $q_0 = -0.5$. For the BAT + XRT dataset, we found that the best fit in all single spectra is given by an absorbed black-body plus a power law with an exponential cut-off, in agreement with the results of Campana et al. (2006). The results of the time-resolved spectral analysis of the two datasets are shown in Tables 1 and 2, while in Fig. 2 we report as an example the best-fit for the *Swift*-BAT+XRT spectrum 5 using a function composed of an

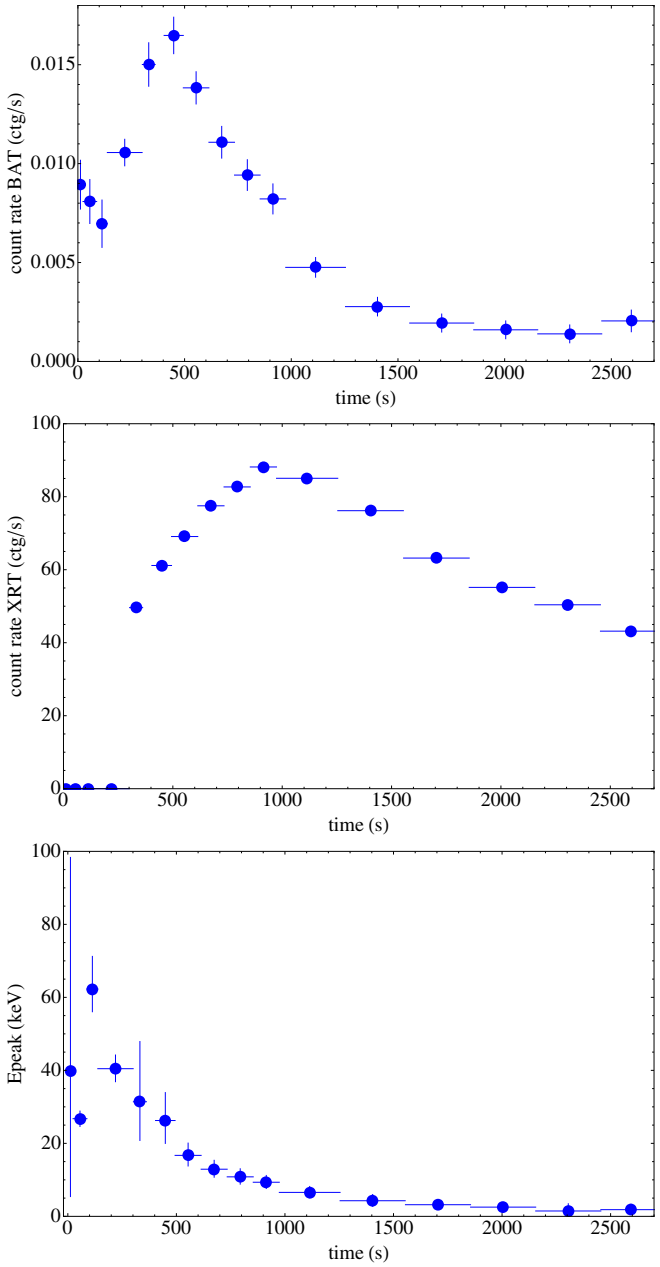

Fig. 2. Net count rate as detected by *Swift*-BAT (15–150 keV; *upper panel*) and by *Swift*-XRT (0.3–10 keV; *middle panel*) after pileup correction. *Lower panel*: variation of the intrinsic peak energy of GRB 060218 as detected by *Swift*.

absorbed black-body plus a power law with an exponential energy cut-off.

The last step consists of computing the integrated spectrum of GRB 060218. We obtained integrated spectra for both datasets using the `mathpha` task, which is provided within the `heasoft` package for data analysis[1]. We then fitted the integrated spectra considering a cut-off power law for the first dataset and an absorbed cut-off power law (Band 2003) plus a black body for the second dataset, obtaining results that are very similar to those presented in Campana et al. (2006). We fixed the galactic column density to the value $N(H_{\rm gal}) = 1.42 \times 10^{21}$ cm^{-2} (see Dickey & Lockman 1990), while for the extragalactic column density, we chose the median of the densities obtained in the

[1] http://heasarc.gsfc.nasa.gov/lheasoft

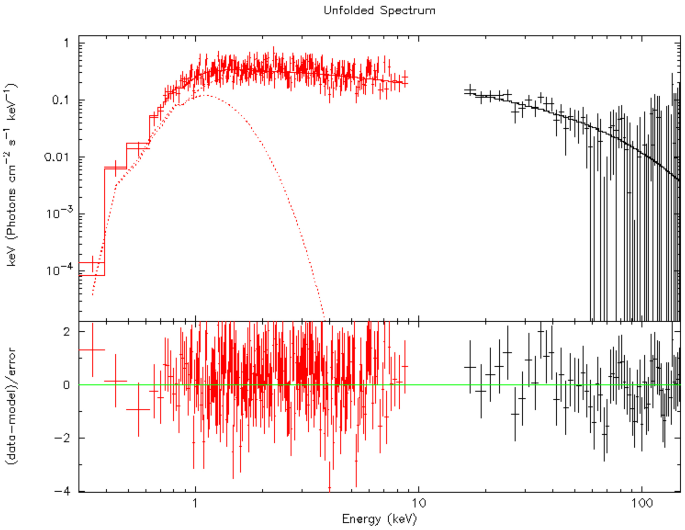

Fig. 3. Best-fit of the *Swift*-BAT+XRT spectrum number 5 (see Table 2) obtained with an absorbed blackbody and a power-law with an exponential energy cutoff function.

different spectra into which our dataset is divided: $N(H_{\rm intr}) = 3.58 \times 10^{21}$ cm^{-2}. The results of the fits are shown in Table 2. From these results, we have computed the values for the intrinsic peak energy $E_{\rm p,i}$ and isotropic energy emitted in the time intervals corresponding to the two datasets, and the evolution of $E_{\rm p}$ is shown in Fig. 2. Finally, we compute the total integrated $E_{\rm p,i}$ and $E_{\rm iso}$ values for *Swift*, by considering a Band function alone and we obtain $E_{\rm p,i,D2} = 4.92 \pm 0.57$ keV and $E_{\rm iso,D2} = (3.10 \pm 0.10) \times 10^{49}$ erg.

2.2. GRB 100316D

GRB 100316D was also discovered by *Swift* (Stamatikos et al. 2010) in the environment of an extended galaxy at the redshift $z = 0.059$ (Vergani et al. 2010). The initial BAT and XRT light curves were very similar to the observed emission of GRB 060218 (Sakamoto et al. 2010) and a thermal component was also observed in X-rays (Starling et al. 2012), although its presence has not been confirmed (Margutti et al. 2013). An SN associated with the burst was also discovered a few days after the GRB discovery when its luminosity was still increasing (Chornock et al. 2010; Bufano et al. 2012). The similarity between the temporal and spectral properties of GRB 100316D with those of GRB 060218, makes GRB 100316D an additional test bed for our purposes. Its T_{90} spectrum, however, is best fitted in the 15−150 keV energy range by a simple power-law function with photon index $\gamma = -2.56 \pm 0.18$. We then derive that this GRB is extremely soft, with a peak energy below the lower energy threshold of *Swift*-BAT ($E_{\rm p,i} \leq 15$ keV). In analogy with GRB 060218, we considered the luminous X-ray tail for the computation of the $E_{\rm p,i}$ and $E_{\rm iso}$ parameters. However, XRT started to observe GRB 100316D only 144 s after the *Swift*-BAT trigger, and 297 s after the first emission observed by BAT, see Fig. A.2.

In order to build an integrated spectrum including both BAT and XRT data, we simulated the XRT emission in the time interval ($T_0 - 153$, T_0+144) s, using the `fakeit` package available in the HEAsoft software packages, and considering the best fit found for the BAT spectrum. After obtaining an XRT spectrum for the first *Swift* orbit using the same procedure as described in the previous section, we computed a total integrated

Table 1. *Swift*-BAT (15−150 keV) spectral fits data results of the first dataset of GRB 060218, that includes the first four BAT spectra (Δt_{D1} = 340 s).

#	Δt (s)	γ	E_{cutoff} (keV)	Norm Photons keV^{-1} cm^{-2} s^{-1}	Flux (10^{-9} erg/cm^2/s)	χ^2/d.o.f.
1	64	$2.07^{+0.44}_{-0.38}$	–	$6.6^{+2.6}_{-2.2} \times 10^{-3}$	5.0	63.2/56
2	64	$2.61^{+0.43}_{-0.37}$	–	$9.6^{+2.9}_{-2.5} \times 10^{-3}$	4.3	59.6/56
3	49	$2.55^{+0.66}_{-0.51}$	–	$7.2^{+3.1}_{-2.5} \times 10^{-3}$	3.4	43.0/56
4	163	$0.91^{+0.85}_{-1.07}$	$35.9^{+3.2}_{-3.0}$	$9.9^{+0.95}_{-0.95} \times 10^{-2}$	5.1	26.2/55

Table 2. *Swift*-BAT+XRT (0.3−150 keV) spectral fit data results of the second dataset of GRB 060218, which includes the last 12 spectra (Δt_{D2} = 2387 s).

#	Δt (s)	γ	E_{cutoff} (keV)	Norm CPO Photons keV^{-1} cm^{-2} s^{-1}	kT (keV)	Norm BB 10^{37} erg s^{-1}	Flux BAT (10^{-9}) (erg/cm^2/s)	Flux XRT (10^{-9}) (erg/cm^2/s)	χ^2/d.o.f.
5	60	$1.36^{+0.11}_{-0.12}$	47^{+23}_{-13}	$0.51^{+0.07}_{-0.07}$	$0.197^{+0.033}_{-0.030}$	$1.23^{+0.30}_{-0.33}$	7.0	3.7	277.8/281
6	90	$1.361^{+0.067}_{-0.078}$	$39.7^{+10.8}_{-8.2}$	$0.68^{+0.05}_{-0.06}$	$0.171^{+0.023}_{-0.017}$	$1.19^{+0.34}_{-0.33}$	7.7	4.7	391.9/412
7	120	$1.290^{+0.065}_{-0.070}$	$22.8^{+4.1}_{-3.3}$	$0.80^{+0.05}_{-0.05}$	$0.151^{+0.018}_{-0.016}$	$1.67^{+0.47}_{-0.38}$	5.5	5.5	398.3/505
8	120	$1.159^{+0.084}_{-0.090}$	$14.9^{+2.4}_{-2.0}$	$0.80^{+0.06}_{-0.07}$	$0.177^{+0.017}_{-0.016}$	$2.05^{+0.35}_{-0.32}$	4.1	6.1	491.6/527
9	120	$1.244^{+0.082}_{-0.088}$	$13.9^{+2.4}_{-2.0}$	$0.96^{+0.07}_{-0.07}$	$0.169^{+0.017}_{-0.016}$	$2.12^{+0.40}_{-0.36}$	3.3	6.2	553.9/539
10	120	$1.225^{+0.082}_{-0.089}$	$11.7^{+2.0}_{-1.7}$	$1.06^{+0.07}_{-0.07}$	$0.162^{+0.015}_{-0.014}$	$2.47^{+0.41}_{-0.41}$	2.7	6.6	461.5/542
11	280	$1.296^{+0.065}_{-0.072}$	$9.0^{+1.3}_{-1.2}$	$1.19^{+0.05}_{-0.05}$	$0.150^{+0.008}_{-0.008}$	$2.98^{+0.37}_{-0.34}$	1.3	6.0	717.9/670
12	300	$1.15^{+0.18}_{-0.23}$	$4.9^{+1.7}_{-1.2}$	$1.15^{+0.05}_{-0.06}$	$0.153^{+0.007}_{-0.007}$	$3.67^{+0.39}_{-0.38}$	2.6	4.7	727.2/631
13	300	$0.80^{+0.21}_{-0.22}$	$2.57^{+0.50}_{-0.37}$	$1.09^{+0.06}_{-0.06}$	$0.152^{+0.006}_{-0.006}$	$4.58^{+0.36}_{-0.35}$	0.023	3.4	570.0/566
14	300	$1.33^{+0.22}_{-0.23}$	$3.67^{+1.21}_{-0.75}$	$1.02^{+0.06}_{-0.06}$	$0.145^{+0.005}_{-0.005}$	$5.20^{+0.43}_{-0.43}$	0.038	2.7	583.9/528
15	300	$1.74^{+0.27}_{-0.27}$	$5.5^{+4.6}_{-1.7}$	$0.95^{+0.06}_{-0.06}$	$0.147^{+0.005}_{-0.005}$	$5.58^{+0.48}_{-0.51}$	0.060	2.3	475.1/488
16	277	$1.49^{+0.31}_{-0.32}$	$3.45^{+1.79}_{-0.90}$	$0.80^{+0.06}_{-0.06}$	$0.144^{+0.004}_{-0.004}$	$5.97^{+0.46}_{-0.48}$	0.014	1.9	519.1/430

spectrum for both detectors by using the `mathpha` package, which is also available in the HEAsoft suite. The fit of this latter spectrum, with a total exposure time of 891 s, is best fit with an absorbed power-law with an exponential cut-off at $E_{cut} = 18.7^{+1.1}_{-1.0}$ keV and a photon index of $\gamma = -1.26^{+0.02}_{-0.02}$, see also Fig. A.1. With these values, we estimate an intrinsic peak energy of $E_{p,i} = 14.69^{+0.94}_{-0.89}$ keV and an isotropic energy of $E_{iso} = 4.841^{+0.026}_{-0.025} \times 10^{49}$ erg, which implies that GRB 100316D satisfies the Amati relation although its location is borderline (see Fig. 7). Finally, we built three distinct time-resolved spectra that we used for the simulation with other detectors. The details of these three time-resolved spectra are shown in Table A.1.

2.3. GRB 161219B

GRB 161219B has been discovered by *Swift*-BAT (D'Ai et al. 2016) and by Konus WIND (Frederiks et al. 2016). Its redshift has been identified two days later (Tanvir et al. 2016) to be $z = 0.1475$, while the emerging SN was observed 7.24 days after the initial trigger (de Ugarte Postigo et al. 2016). The T_{90} duration observed by *Swift*-BAT is 6.9 s, but a more detailed analysis of BAT data revealed an extended emission, lasting ∼20 s, anticipating the burst (Palmer et al. 2016), as well as a tail lasting up to 40 s from the GRB trigger, see Fig. A.3. *Swift* XRT started to observe this GRB only 108 s after the BAT trigger (D'Ai et al. 2016), therefore we do not have a continuity in the observations between BAT and XRT for this GRB.

The T_{90} spectrum of this GRB, as observed by *Swift*-BAT, is best fitted by a power-law function with an exponential cut-off at $E_0 = 92.3^{+68.2}_{-29.0}$ keV and a photon index of $\gamma = -1.40^{+0.23}_{-0.24}$ (Cano et al. 2017). The corresponding intrinsic peak energy is $E_{p,i} = 62.3^{47.0}_{-19.9}$ keV and the isotropic energy $E_{iso} = 8.50^{+8.46}_{-3.75} \times 10^{49}$ erg, in the 1−10 000 keV energy range. With these values, the location of GRB 161219B is within three sigma of the Amati relation, while when we consider the data provided by the Konus-WIND mission (Frederiks et al. 2016), this burst would not satisfy the correlation at all, see Fig. 1.

In order to obtain more reliable values of the average $E_{p,i}$ and E_{iso} of the whole event, we repeated the analysis by also including the first soft/weak pulse and the soft tail described previously and shown in Fig. A.3. The BAT data were downloaded, screened, and analysed by following the standard procedures[2] and using the usual HEASOFT packages. The total spectrum is best fitted by a Band function (Band et al. 1993) with the following parameters: $\alpha = -1.14^{+0.16}_{-0.13}$, $\beta = -2.37^{+0.52}_{-1.59}$, and

[2] The *Swift*-BAT data analysis is described at https://swift.gsfc.nasa.gov/analysis/

$E_{p,i} = 55.5^{+14.9}_{-8.9}$ keV. The total integrated isotropic energy in the 1−10 000 keV energy range is $E_{iso} = 1.83 \times 10^{51}$ erg, which places this GRB well inside the limits of the Amati relation. Finally, we obtained and analysed four time-resolved spectra from the total emission of GRB 161219B, to be used in the simulations with other detectors. Figure A.3 clearly shows that we have extracted two single spectra from the GRB main pulse and an additional two spectra for the precursor and the soft tail. The best-fit results of the *Swift*-BAT data for each single spectrum are shown in Table A.2.

3. Simulated observations with other detectors

After deriving the spectral emission of the GRBs 060218, 100316D and 161219B as observed by *Swift*, we simulated observing them with old instruments dedicated to GRB observations, such as *Beppo*SAX, BATSE, INTEGRAL, and with a planned instrument that is very sensitive to soft X-ray frequencies, that is, the Wide Field Monitor (WFM).

The energy range of *Beppo*SAX (see Frontera et al. 2000) was very wide: from 2 keV to about 700 keV. This broad range was obtained thanks to two distinct detectors: the Wide Field Camera (WFC; Jager et al. 1997) which operated between 2 and 30 keV and the Gamma Ray Burst Monitor (GRBM; Frontera et al. 1997), whose energy range was 40−700 keV. We here only considered the GRBM detector because it was the GRB alert detector on board *Beppo*SAX. The BATSE Large Area Detector (LAD) was an experiment on board the Compton Gamma-Ray Observer (CGRO), and it consisted of eight detector module of NaI(TI), covering a wide energy range from 20 keV to 2 MeV. An interesting feature of the BATSE-LAD was that the location of these eight detectors allowed to cover a very wide fraction of the sky, $\Omega = 4\pi$. The INTErnational Gamma-Ray Astrophysics Laboratory (INTEGRAL) is a facility designed to investigate high-energy objects, carrying detectors for the X-ray and gamma-ray part of the spectrum, with an energy of between 15 keV and 10 MeV (Mereghetti et al. 2003). eXTP (Zhang et al. 2016) is a proposed mission for timing analysis of the X-ray transient sky and is expected to also mount a wide field monitor instrument that is able to detect GRBs in the energy range 2−70 keV (Feroci et al. 2012).

The time-resolved spectral best fits obtained in Sect. 2 (see also Tables 1, 2, A.1, and A.2) represent our input spectral models in the simulated observations. We used the standard `fakeit` procedure within the XSPEC package to simulate the observed spectra for all instruments, which requires correct background and a spectral response matrix for all detectors, plus an additional ancillary response file for the WFM and INTEGRAL cases. We obtained the response matrices, background, and ancillary files for each detector from the specific web sites[3] or from the literature (Kaneko et al. 2006; Guidorzi et al. 2011).

Before spectral fitting, we grouped any spectra to have a number of ten counts per bin, using the `grppha` tool of the `heasoft` package. Then, we used XSPEC to find the best model of each single time-resolved simulated spectrum, as if the GRB was really observed by the considered detector.

However, in order to obtain the total integrated spectrum and given the different sensitivities of the four detectors, we needed

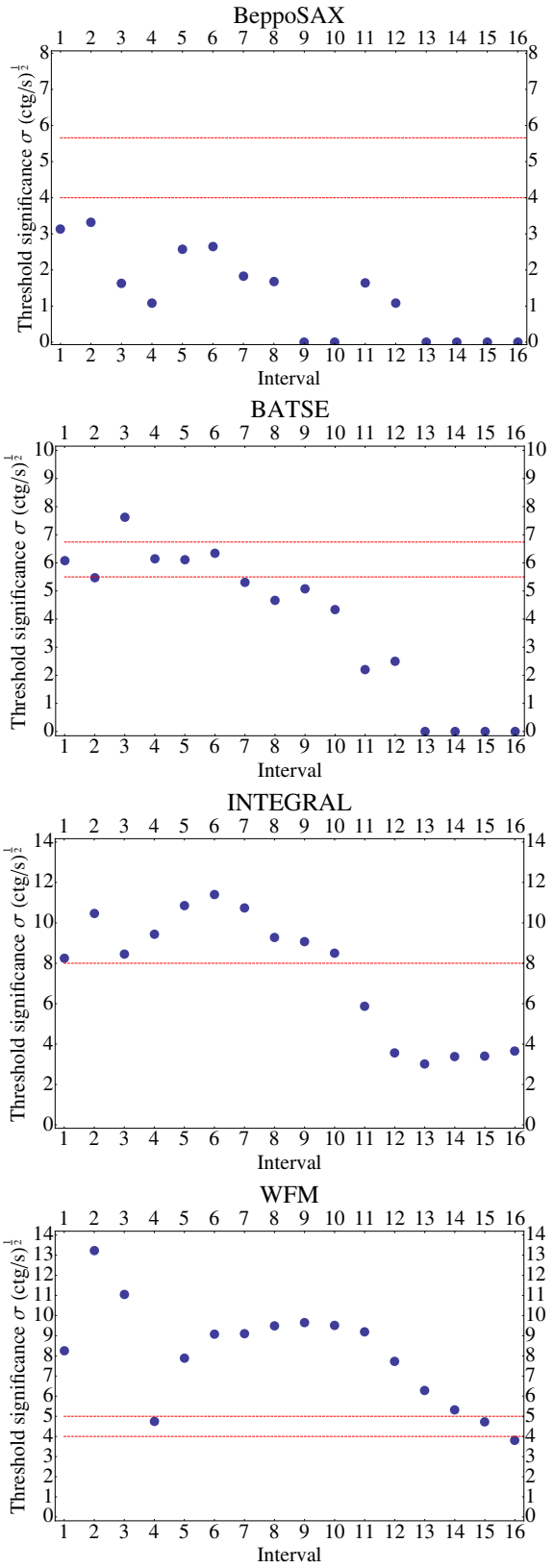

Fig. 4. Threshold significance σ as a function of the interval for *Beppo*SAX, BATSE, INTEGRAL, and WFM. The red, horizontal lines represent the σ_0 threshold as calculated from 1 (see also Band et al. 1993). In the case of *Beppo*Sax, BATSE, and WFM, we report two horizontal lines because the value of the threshold σ_0 depends on the angle between the direction perpendicular to the plane of the detector and the direction of the source. We use the lower value throughout the whole analysis.

[3] http://www.isdc.unige.ch/extp/public-response-files.html
http://saxgrbm.iasfbo.inaf.it/
http://heasarc.gsfc.nasa.gov/W3Browse/cgro/batsegrbsp.html

Table 3. Time-integrated spectral fit results for the observed *Swift* data and for the simulated spectra of GRB 060218.

# (keV)	Δt (s)	α (γ)	$E_{\rm p,i}$ (keV)	Norm # keV^{-1} cm^{-2} s^{-1}	χ^2/d.o.f.	$E_{\rm iso}$ (10^{49} erg)
Swift (BAT+XRT) (0.3–150)	2383	$-1.178^{+0.061}_{-0.062}$	$4.62^{+0.60}_{-0.54}$	$0.935^{+0.017}_{-0.017}$	1083.0/871	$5.35^{+0.53}_{-0.53}$
Swift (BAT) (15–150)	2727	$-0.72^{+0.19}_{-0.12}$	$21.3^{+3.1}_{-3.5}$	$4.8^{+2.1}_{-2.1}\times10^{-3}$	1.4/57	$1.23^{+0.12}_{-0.11}$
INTEGRAL (15–200)	971	$-1.81^{+0.036}_{-0.032}$	$8.4^{+2.3}_{-2.0}$	$1.91^{+0.20}_{-0.20}$	0.25/34	$3.420^{+0.023}_{-0.020}$
BATSE (25–1900)	490	$-1.213^{+0.091}_{-0.067}$	$33.3^{+8.3}_{-7.6}$	$0.032^{+0.095}_{-0.095}$	109.1/112	$1.268^{+0.027}_{-0.024}$
eXTP-WFM (2–50)	2450	$-1.831^{+0.012}_{-0.012}$	$4.19^{+0.46}_{-0.42}$	$1.28^{+0.024}_{-0.024}$	346.8/476	$4.861^{+0.015}_{-0.014}$

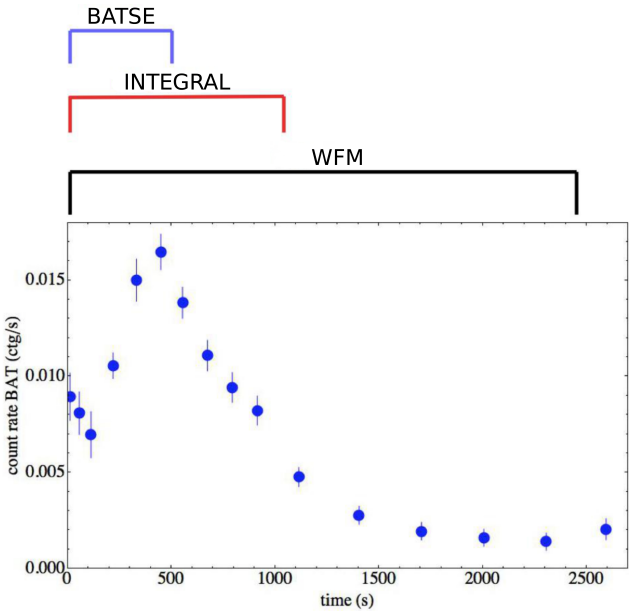

Fig. 5. Light curve of GRB 060218 as observed by *Swift*-BAT compared with the effective emission observed by *Beppo*SAX, BATSE, and WFM.

to consider the effective duration of each GRB emission as observed by each single detector. For this reason we computed the threshold significance σ for any single simulated time-resolved spectrum and for each detector in order to determine the real duration of the GRB. Following Band (2003), the threshold significance is given by

$$\sigma_0 = \frac{A_{\rm eff} f_{\rm det} f_{\rm mask} \Delta t \int_{E_1}^{E_2} \epsilon(E) N(E) {\rm d}E}{\sqrt{A_{\rm eff} f_{\rm det} \Delta t \int_{E_1}^{E_2} B(E) {\rm d}E}}, \quad (1)$$

where $A_{\rm eff}$ is the effective area of the detector, $f_{\rm det}$ is the fraction of the detector plane that is active, $f_{\rm mask}$ is the fraction of the coded mask that is open, Δt is the exposure of the photon spectrum $N(E)$, $\epsilon(E)$ is the efficiency of the detector, and $B(E)$ is the background. E_1 and E_2 correspond to the minimum and maximum energy threshold for any detector considered in this analysis.

As final results, we obtained different time intervals for each detector in which the burst would trigger it, and the intervals also provide a signal with a sufficient number of counts to be analysed with XSPEC, see Fig. 4 for the case of GRB 060218: while *Beppo*SAX would not have been triggered at all, WFM would have missed only the last 277 s, and BATSE and INTEGRAL would have seen the first 490 s and 971 s, respectively.

Table 4. Redshift, $E_{\rm peak}$, and $E_{\rm iso}$ values obtained from *Swift* observations.

Event	Redshift (z)	$E_{\rm iso}$ (10^{52} erg)	$E_{\rm peak}$ (keV)
GRB 060908	1.88	$7.2^{+1.9}_{-1.9}$	553^{+260}_{-260}
GRB 060927	5.46	$12.0^{+2.8}_{-2.8}$	275^{+75}_{-75}
GRB 140206A	2.74	$36.806^{+0.058}_{-0.058}$	$364.4^{+4.7}_{-4.6}$
GRB 141220A	1.34	$1.6136^{+0.0098}_{-0.0095}$	265^{+12}_{-11}
GRB 151029A	2.74	$8.013^{+0.069}_{-0.068}$	$117.6^{+4.1}_{-4.1}$
GRB 160227A	2.38	$5.924^{+0.039}_{-0.038}$	248^{+15}_{-14}
GRB 161117A	1.55	$14.858^{+0.018}_{-0.018}$	$145.2^{+1.2}_{-1.2}$
GRB 170113A	1.97	$0.7299^{+0.0053}_{-0.0052}$	$200.9^{+9.1}_{-8.8}$

We then computed the time-integrated spectra for each detector by summing with `mathpha` the spectra with a positive detection and then obtained the best fit for each of them, which were a cut-off power law in every case.

After we calculated the $E_{\rm peak}$ from the simulated spectra, we estimated the relative $E_{\rm iso}$ by first calculating the corresponding bolometric fluence $S_{\rm bolo}$ using the relation (see Schaefer 2007):

$$S_{\rm bolo} = S_{\rm obs} \frac{\int_{\frac{1}{1+z}}^{\frac{10^4}{1+z}} E\phi {\rm d}E}{\int_{E_{\rm min}}^{E_{\rm max}} E\phi {\rm d}E}, \quad (2)$$

where Φ is the differential photon spectrum (dN/dE) and $S_{\rm obs}$ is the observed fluence calculated from the spectrum, z is the redshift and $E_{\rm min}$ and $E_{\rm max}$ are the extremes of the detector bandpass. For GRB 060218, we report the result of our calculation in Fig. 6 and Table 3: while the location estimated with WFM matches the Amati relation, the locations obtained with BATSE and INTEGRAL do not match it. In the same figure we also report the location of GRB 060218 as observed by *Swift*-BAT+XRT (060218 *Swift*). On the basis of all these results, we conclude that these different locations in the $E_{\rm p,i} - E_{\rm iso}$ plane of GRB 060218 as observed by BATSE and INTEGRAL are due to their lack of a highly sensitive soft X-ray detector capabilities.

Similar conclusions are drawn for the cases of GRB 100316D and GRB 161219B. These events show an extended soft emission similar to that of GRB 060218, although GRB 161219B shows a higher energy output, enabling us to explore a different region of the $E_{\rm peak}/E_{\rm iso}$ plane in search of a bias effect. The results of our spectral analysis are reported in Tables A.1 and A.2, while the positions on the $E_{\rm peak}/E_{\rm iso}$ plane of these two events according to the different detectors we considered are reported in Fig. 7. GRB 161219B is an outlier of the Amati relation

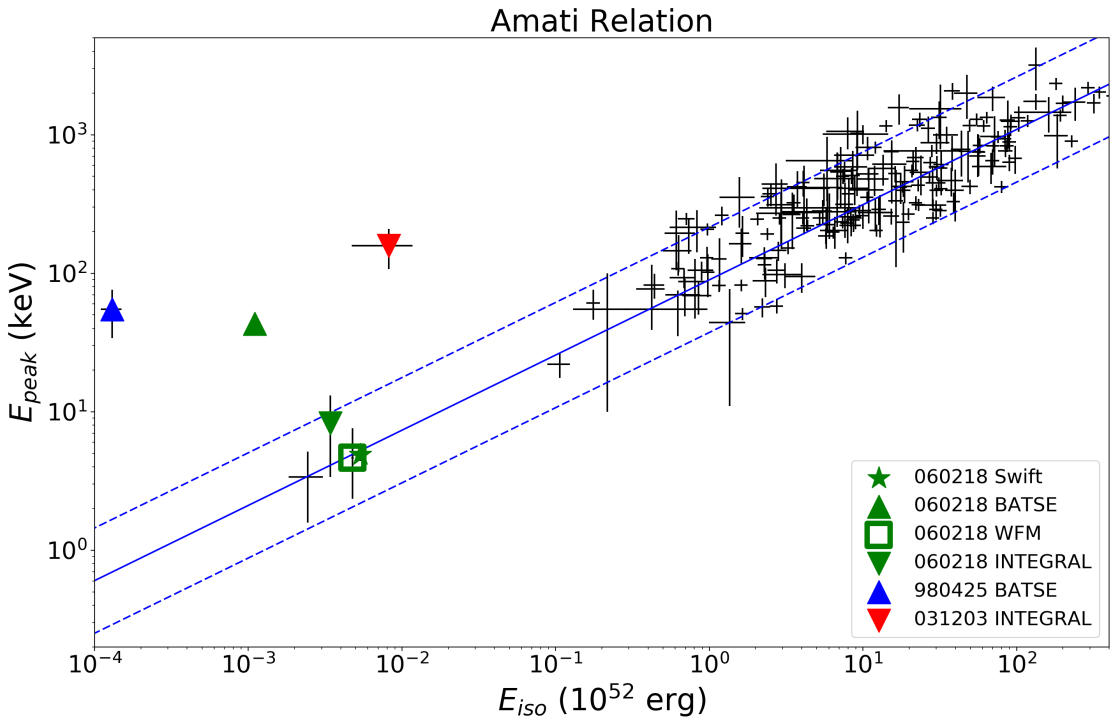

Fig. 6. $E_{p,i}$ – E_{iso} plane (Amati relation). We report in green the position of GRB 060218: according to *Swift* (BAT+XRT) (star), as it would have been observed by BATSE (triangle), INTEGRAL (reverse triangle) and WFM (square). We also show the location in the $E_{p,i}$ – E_{iso} plane of the two outliers GRB 980425 (blue triangle) and GRB 031203 (red reverse triangle).

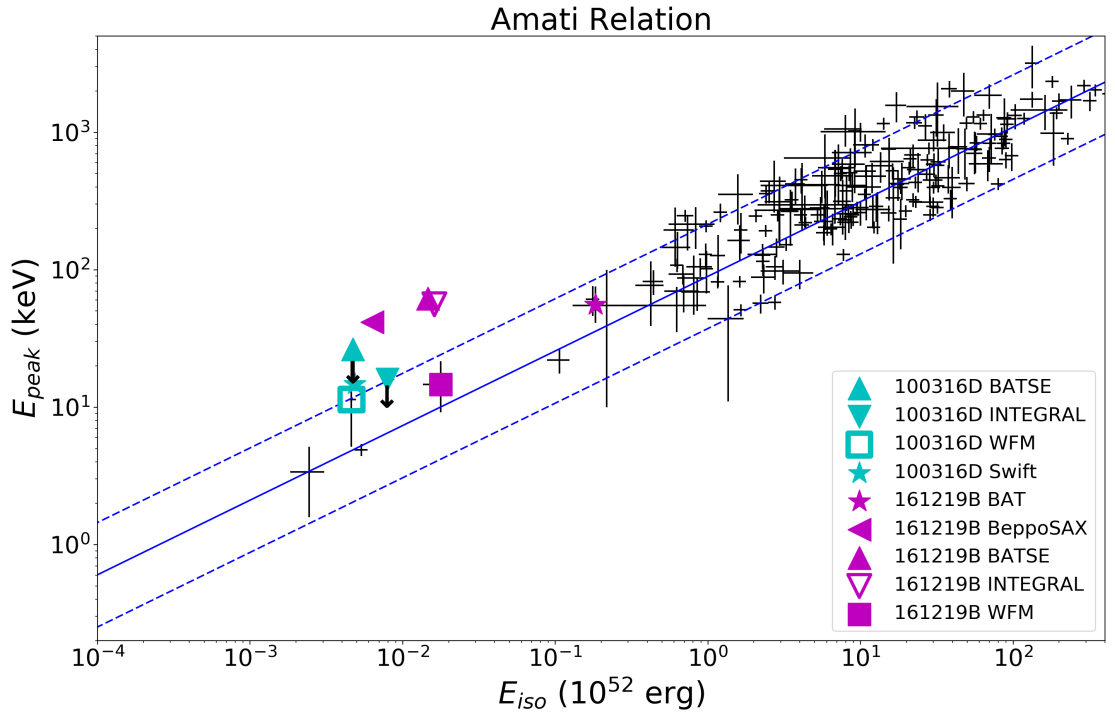

Fig. 7. $E_{p,i}$ – E_{iso} plane (Amati relation). We report in cyan the position of GRB 100316D: according to *Swift* (BAT+XRT) (star), as it would have been observed by BATSE (triangle – upper limit), INTEGRAL (reverse triangle – upper limit) and WFM (square). We also show the location of GRB 161219B: according to *Swift* (BAT) (star), *Beppo*SAX (left triangle), BATSE (triangle), INTEGRAL (reverse triangle), and WFM (square – upper limit).

for all the detectors considered in this work, with the exception of the eXTP-WFM, while only BATSE would have measured GRB 100316D to lie outside the Amati relation (but with an unconstrained lower limit for the $E_{p,i}$ value).

As a countercheck to our result, we applied our approach to a set of eight cosmological bursts ($z > 0.1$), reported in Table 3, whose $E_{p,i}$ and E_{iso} have been measured by *Swift*-BAT and perfectly match the Amati relation (see Fig. 8). We

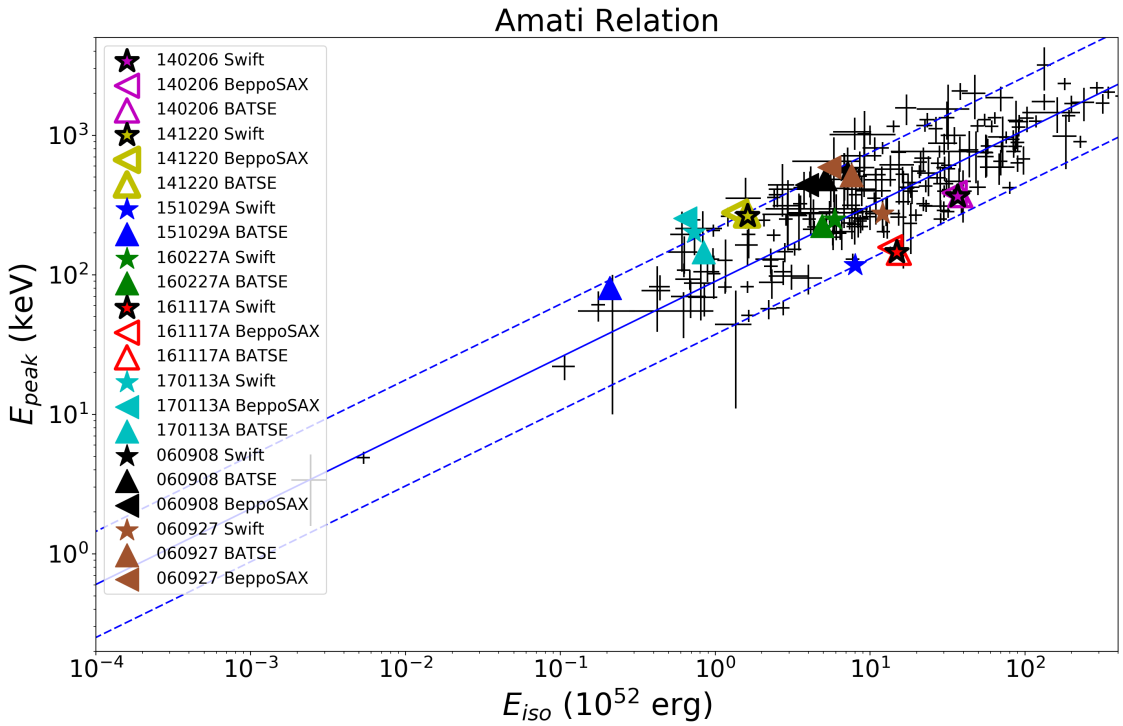

Fig. 8. Positions in the $E_{p,i} - E_{iso}$ plane of the eight cosmological GRBs, described in the text, characterized by a higher energy and a higher redshift than GRB 060218, GRB 161219B, and GRB 100316D. We note that the emission of these events as observed by BATSE and *Beppo*-SAX still satisfies the $E_{p,i} - E_{iso}$ correlation.

Table 5. Time-integrated spectral fit results for the observed *Swift* data and for the simulated spectra of GRB 100316D.

# (keV)	Δt (s)	α (γ)	$E_{p,i}$ (keV)	Norm # keV^{-1} cm^{-2} s^{-1}	χ^2/d.o.f.	E_{iso} (10^{49} erg)
Swift (BAT+XRT) (0.3–150)	890	$-1.256^{+0.018}_{-0.018}$	$14.69^{+0.94}_{-0.89}$	$0.4446^{+0.0053}_{-0.0053}$	568.7/971	$4.841^{+0.026}_{-0.025}$
INTEGRAL (15–200)	497	$-2.38^{+0.26}_{-0.23}$	15.9	$4.9^{+6.1}_{-2.6}$	1.8/35	$7.91^{+0.92}_{-0.51}$
BATSE (25–1900)	200	$-2.358^{+0.059}_{-0.047}$	26.5	$6.9^{+1.5}_{-1.5}$	102/113	$4.722^{+0.104}_{-0.097}$
eXTP-WFM (2–50)	891	$-1.62^{+0.14}_{-0.14}$	$11.4^{+17.7}_{-6.2}$	$0.710^{+0.084}_{-0.041}$	415/476	$4.61^{+0.33}_{-0.14}$

Table 6. Time-integrated spectral fit results for the observed *Swift* data and for the simulated spectra of GRB 161219B.

# (keV)	Δt (s)	α (γ)	$E_{p,i}$ (keV)	Norm # keV^{-1} cm^{-2} s^{-1}	χ^2/d.o.f.	E_{iso} (10^{49} erg)
Swift (BAT) (15–150)	62	$-1.435^{+0.050}_{-0.042}$	$56^{+20}_{-14.0}$	$20.1^{+3.4}_{-3.4}$	1.2/55	$183^{+5.1}_{-4.2}$
*Beppo*SAX (40–700)	8	$-1.46^{+0.60}_{-0.72}$	$41.5^{+1.9}_{-1.9}$	$13.44^{+0.76}_{-0.76}$	339/223	$6.328^{+0.039}_{-0.038}$
INTEGRAL (15–200)	62	$-1.5304^{+0.0059}_{-0.0058}$	$56.0^{+3.4}_{-3.2}$	$2.1506^{+0.0059}_{-0.0058}$	5.9/34	$16.127^{+0.060}_{-0.057}$
BATSE (25–1900)	62	$-1.336^{+0.013}_{-0.012}$	$61.8^{+3.8}_{-3.6}$	$1.202^{+0.063}_{-0.063}$	38.15/112	$1.465^{+0.100}_{-0.097}$
eXTP-WFM (2–50)	62	$-1.7297^{+0.0053}_{-0.0051}$	$14.7^{+3.6}_{-4.2}$	$1.173^{+0.023}_{-0.023}$	475/478	$17.72^{+0.36}_{-4.15}$

performed time-integrated simulations for the BATSE-LAD and *Beppo*SAX-GRBM instruments using the observed dataset from *Swift*. The simulated points in the $E_p - E_{iso}$ plane are reported in Fig. 8. According to our analysis, we do not see a strong effect/bias for these events in these cases. All these GRBs are consistent with the $E_{p,i} - E_{iso}$ correlation, even if they would have been observed by BATSE-LAD and *Beppo*SAX-GRBM. This result implies that this effect is strong only for sub-energetic events and with a soft X-ray prolonged emission.

We note that during the complete duration of the prompt emission, the value of the peak energy is almost in the energy interval 2–70 keV (see Fig. 2), which is the nominal energy range of the Wide Field Monitor proposed for the LOFT (Feroci et al. 2012) and eXTP (Zhang et al. 2016) mission concepts. Its sensitivity, with respect to other current and past GRB detectors, is almost one order of magnitude higher[4], suggesting that events similar to GRB 060218 could also be detected at larger distances

[4] http://sci.esa.int/loft/53447-loft-yellow-book/

($z \approx 0.1-0.2$). It is therefore interesting to estimate the cosmological region of the Universe in which we can detect low-luminosity GRBs-SNe with WFM and, eventually, provide an estimate of the rate of such events. We therefore estimated the maximum distance at which GRB 060218-like bursts would still trigger the eXTP-WFM. A positive trigger of eXTP-WFM depends on the assumed threshold significance, defined in Eq. (1), but we also need to correct the observed spectrum there because the assumed distance of the GRB is different. We specifically modified:

- the exposure time Δt_z, which varies as $\Delta t_{\rm rest}(1+z)$, where $\Delta t_{\rm rest}$ corresponds to the observed time interval in the rest frame: $\Delta t_{\rm rest} = \Delta t_{\rm obs}/1.0331$;
- the cut-off energy $E_{\rm cutoff}$, which is parameterized as the peak energy E_p, and which varies as $E_{\rm cutoff,z} = E_{\rm cutoff,obs}\frac{1.0331}{1+z}$;
- the normalization of the spectral model, which varies following the functional form:

$$K_z = K_{\rm obs}\left(\frac{1+z}{1.0331}\right)^2\left(\frac{d_l(0.0331)}{d_l(z)}\right)^2. \quad (3)$$

We note that the subscripts *obs* correspond to the quantities observed by *Swift* and the subscript z to the quantities that would be observed if GRB 060218 were to remain at redshift z. With these corrections, we computed the threshold significance σ for the time-resolved spectrum 6 in Fig. 5, which is the spectrum with the highest expected σ and does not belong to the initial hard emission of GRB 060218, translated into different redshifts. Assuming a value of $\sigma = 4$ for the eXTP-WFM, which is the expected final value for the mission, we obtain that an event similar to GRB 060218 would trigger the WFM up to a redshift $z = 0.1$, see also Fig. A.4.

We also determined at which redshift GRB 060218 would have been observed by *Swift*-BAT, and we obtained a redshift of $z = 0.05$ as the detection limit for GRB 060218 with *Swift*-BAT. The cosmological comoving element volume at redshift z is given by

$$V(z) = \frac{4\pi}{3}d_{\rm c}(z)^3, \quad (4)$$

where $d_{\rm c} = d_l/(1+z)$ is the cosmological comoving distance. At these distances ($z = 0.1$), the comoving element volume is 30 times larger than the volume at $z = 0.0331$ and 8 times larger than the volume at $z = 0.05$.

4. Conclusions

The main results of our analysis can be summarized as follows:

i) If GRB 060218, 161219B, and 100316D were observed with detectors not sensitive at low energies (~0.3 keV) such as INTEGRAL and/or BATSE, they would be outliers of the Amati relation (see Amati & Dichiara 2013, for a quantitative analysis of the instrumental bias). On the other hand, GRB 060218 and GRB 100316D perfectly match the $E_{\rm p,i} - E_{\rm iso}$ relation after being observed with *Swift* (down to 0.3 keV). On the basis of this result, we suggest that GRB 980425 and GRB 031203 are not "true" outliers of the Amati relation, and their location in the $E_{\rm p,i} - E_{\rm iso}$ plane is the result of an observational bias, and is not related to a combination of the geometry of GRB explosions with the line of sight of the observer (e.g. GRB viewed off-axis Yamazaki et al. 2004; Ramirez-Ruiz et al. 2005; Eichler & Levinson 2004).

ii) This conclusion is strengthened by the fact that *Swift*-BAT (15−150 keV) did measure GRB 060218 as an outlier and *XMM-Newton* observed an X-ray echo that suggests the presence of an extended soft emission associated with GRB 031203 (Watson et al. 2006).

iii) In the case of GRB 100316D, we note that the WFM observes it at the border of the 1σ boundary of the Amati relation. We therefore derive that it is not sufficient to observe below the limit of the soft X-rays energy range (~0.3 keV), but it is necessary to use a detector with high sensitivities at these energies, such as *Swift*-XRT, in order to obtain as much information as possible about the total energy emitted by these low-luminosity GRBs.

iv) To give more weight to our conclusions, we applied the same approach to a sample of "high-luminosity" GRBs whose $E_{\rm p,i}$ and $E_{\rm iso}$ parameters, reported in Table 3, have been measured by *Swift*-BAT. All these GRBs are more energetic and located at higher redshift than GRB 060218, GRB 100316D and GRB 161219B, and they are therefore not expected to show a soft X-ray tail. In these cases the GRBs always match the $E_{\rm p,i} - E_{\rm iso}$ relation regardless of whether it is observed by *Swift*, BATSE, or *Beppo*SAX (see Fig. 8).

v) After simulating WFM observations, we showed that GRB 060218 could have been observed up to $z = 0.1$ which is about three times farther than it was observed with *Swift*-BAT (Guetta & Della Valle 2007). As a consequence, we are likely lacking a significant fraction of low-luminosity and sub-energetic GRBs, whose high-energy emission remains undetected due to the poor sensitivity and limits of current operating detectors.

Acknowledgements. This research has made use of data, software and web tools obtained from the High Energy Astrophysics Science Archive Research Center (HEASARC), a service of the Astrophysics Science Division at NASA/GSFC and of the Smithsonian Astrophysical Observatory's High Energy Astrophysics Division. This work made use of data supplied by the UK *Swift* Science Data Centre at the University of Leicester. We thank the anonymous referee for his useful comments and suggestions that improved our paper. We thank Sergio Campana for providing us the *Swift*-BAT spectral dataset of GRB 060218. Special thanks go to Prof. Mauro Orlandini, who contributed to the statistical analysis contained in the work and Cristiano Guidorzi for his useful suggestions. LI7 acknowledges support from the Spanish research project AYA 2014-58381-P. D.G. acknowledges the financial support of the UnivEarthS Labex program at Sorbonne Paris Cité (ANR-10-LABX-0023 and ANR-11-IDEX-0005-02).

References

Amati, L. 2006, MNRAS, 372, 233
Amati, L., & Della Valle, M. 2013, Int. J. Mod. Phys. D, 22, 1330028
Amati, L., & Dichiara, S. 2013, Acta Polytechnica, 53, 686
Amati, L., Frontera, F., Tavani, M., et al. 2002, A&A, 390, 81
Amati, L., Guidorzi, C., Frontera, F., et al. 2008, MNRAS, 391, 577
Amati, L., Del Monte, E., D'Elia, V., et al. 2013, Nucl. Phys. B Proc. Suppl., 239, 109
Arnaud, K. A. 1996, in Astronomical Data Analysis Software and Systems V, eds. G. H. Jacoby, & J. Barnes, ASP Conf. Ser., 101, 17
Band, D. L. 2003, ApJ, 588, 945
Band, D., Matteson, J., Ford, L., et al. 1993, ApJ, 413, 281
Barthelmy, S. D., Barbier, L. M., Cummings, J. R., et al. 2005, Space Sci. Rev., 120, 143
Bernardini, M. G., Margutti, R., Zaninoni, E., & Chincarini, G. 2012, MNRAS, 425, 1199
Bufano, F., Pian, E., Sollerman, J., et al. 2012, ApJ, 753, 67
Burrows, D., Hill, J., Nousek, J., et al. 2005, Space Sci. Rev., 120, 165
Campana, S., Mangano, V., Blustin, A. J., et al. 2006, Nature, 442, 1008
Cano, Z., Izzo, L., de Ugarte Postigo, A., et al. 2017, A&A, 605, A107
Chornock, R., Berger, E., Levesque, E. M., et al. 2010, ArXiv e-prints [arXiv:1004.2262]
D'Ai, A., Kennea, J. A., Krimm, H. A., et al. 2016, GRB Coordinates Network, 20296, 1

Dainotti, M. G., Cardone, V. F., & Capozziello, S. 2008, MNRAS, 391, L79
de Ugarte Postigo, A., Cano, Z., Izzo, L., et al. 2016, GRB Coordinates Network, 20342, 1
Della Valle, M. 2011, Int. J. Mod. Phys. D, 20, 1745
Dickey, J. M., & Lockman, F. J. 1990, ARA&A, 28, 215
Eichler, D., & Levinson, A. 2004, ApJ, 614, L13
Feroci, M., Stella, L., van der Klis, M., et al. 2012, Exp. Astron., 34, 415
Frederiks, D., Golenetskii, S., Aptekar, R., et al. 2016, GRB Coordinates Network, 20323, 1
Frontera, F., Costa, E., dal Fiume, D., et al. 1997, A&AS, 122, 357
Frontera, F., Amati, L., Costa, E., et al. 2000, ApJS, 127, 59
Galama, T. J., Vreeswijk, P. M., van Paradijs, J., et al. 1998, Nature, 395, 670
Ghirlanda, G., Ghisellini, G., & Lazzati, D. 2004, ApJ, 616, 331
Ghisellini, G., Ghirlanda, G., Mereghetti, S., et al. 2006, MNRAS, 372, 1699
Guetta, D., & Della Valle, M. 2007, ApJ, 657, L73
Guidorzi, C., Lacapra, M., Frontera, F., et al. 2011, A&A, 526, A49
Izzo, L., Muccino, M., Zaninoni, E., Amati, L., & Della Valle, M. 2015, A&A, 582, A115
Jager, R., Mels, W. A., Brinkman, A. C., et al. 1997, A&AS, 125, 557
Kaneko, Y., Preece, R. D., Briggs, M. S., et al. 2006, ApJS, 166, 298
Liang, E., & Zhang, B. 2005, ApJ, 633, 611
Margutti, R., Soderberg, A. M., Wieringa, M. H., et al. 2013, ApJ, 778, 18
Mazzali, P. A., Deng, J., Nomoto, K., et al. 2006, Nature, 442, 1018
Meegan, C. A., Fishman, G. J., Wilson, R. B., et al. 1992, Nature, 355, 143
Mereghetti, S., Götz, D., Borkowski, J., Walter, R., & Pedersen, H. 2003, A&A, 411, L291
Nousek, J. A., Kouveliotou, C., Grupe, D., et al. 2006, ApJ, 642, 389
Palmer, D. M., Barthelmy, S. D., Cummings, J. R., et al. 2016, GRB Coordinates Network, 20308, 1
Pian, E., Mazzali, P. A., Masetti, N., et al. 2006, Nature, 442, 1011
Ramirez-Ruiz, E., Granot, J., Kouveliotou, C., et al. 2005, ApJ, 625, L91
Romano, P., Campana, S., Chincarini, G., et al. 2006, A&A, 456, 917
Sakamoto, T., Barthelmy, S. D., Baumgartner, W. H., et al. 2010, GRB Coordinates Network, 10511, 1
Schaefer, B. E. 2007, ApJ, 660, 16
Stamatikos, M., Sakamoto, T., Starling, R. L. C., et al. 2010, GCN Report, 278, 1
Starling, R. L. C., Wiersema, K., Levan, A. J., et al. 2011, MNRAS, 411, 2792
Starling, R. L. C., Page, K. L., Pe'Er, A., Beardmore, A. P., & Osborne, J. P. 2012, MNRAS, 427, 2950
Tanvir, N. R., Kruehler, T., Wiersema, K., et al. 2016, GRB Coordinates Network, 20321, 1
Vergani, S. D., D'Avanzo, P., Malesani, D., et al. 2010, GRB Coordinates Network, 10495, 1
Watson, D., Vaughan, S. A., Willingale, R., et al. 2006, ApJ, 636, 967
Waxman, E., Mészáros, P., & Campana, S. 2007, ApJ, 667, 351
Wilms, J., Allen, A., & McCray, R. 2000, ApJ, 542, 914
Woosley, S. E., & Bloom, J. S. 2006, ARA&A, 44, 507
Yamazaki, R., Yonetoku, D., & Nakamura, T. 2004, in Gamma-Ray Bursts: 30 yr of Discovery, eds. E. Fenimore, & M. Galassi, AIP Conf. Ser., 727, 416
Yonetoku, D., Murakami, T., Nakamura, T., et al. 2004, ApJ, 609, 935
Zhang, S. N., Feroci, M., Santangelo, A., et al. 2016, in Proc. SPIE, 9905, 99051Q

Appendix A: Tables and figures

In this section we report the light curves and the statistical results of the spectral analysis performed on GRB 100316D and GRB 161219B. We use these two events as a further verification of our thesis on the behaviour of the statistical bias we described in the conclusions of our work.

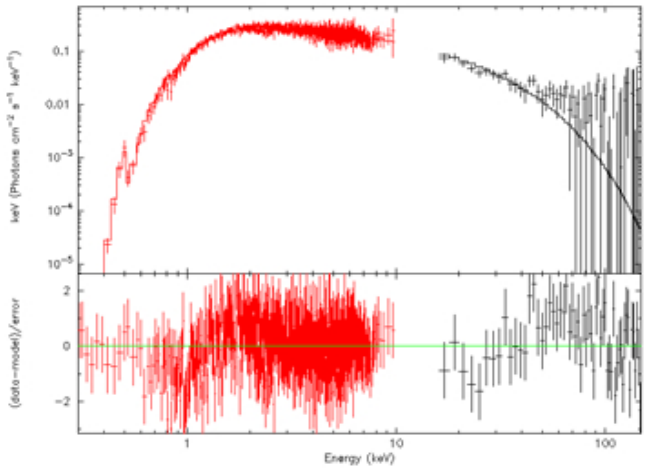

Fig. A.1. Best fit of the *Swift*-BAT+XRT integrated spectrum of GRB 100316D with an absorbed power-law function with an exponential cut-off.

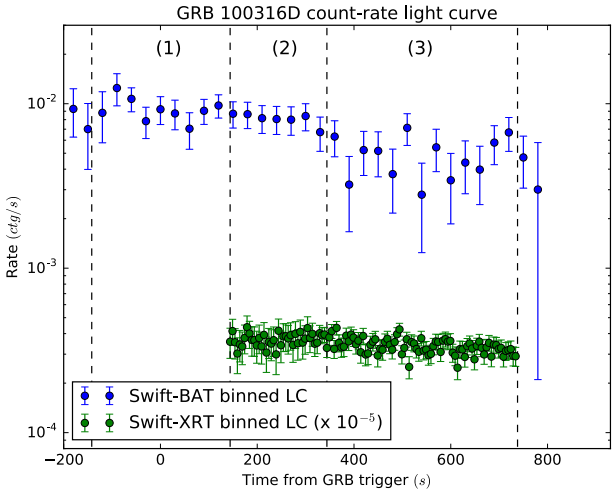

Fig. A.2. *Swift*-BAT (blue circles) and XRT (green circles) count-rate light curve of GRB 100316D. Both curves are binned while the XRT curve is also rescaled by 10^{-5}. The dashed black lines mark the time intervals of the time-resolved spectra considered in our analysis (see also Table A.1).

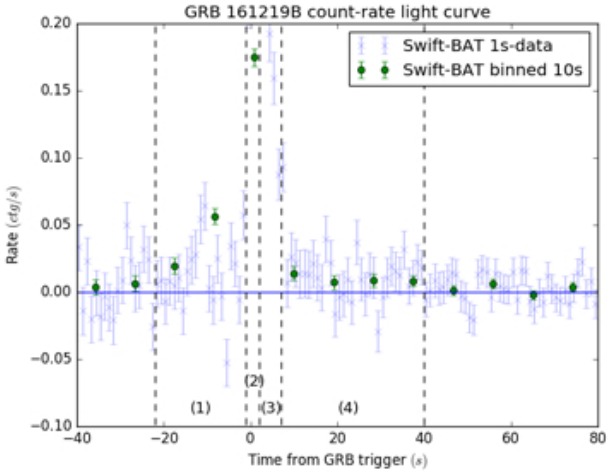

Fig. A.3. *Swift*-BAT count-rate light curve of GRB 100316D binned at 1 s (blue data) and at 10 s (green circles). The dashed black lines mark the time intervals of the time-resolved spectra considered in our analysis (see also Table A.2).

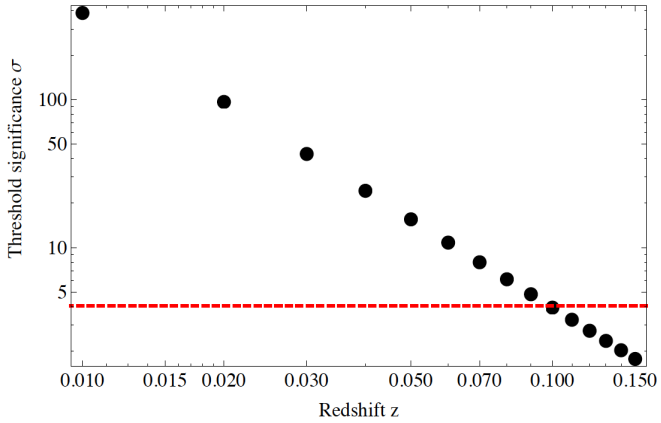

Fig. A.4. eXTP threshold significance for the brightest time-resolved spectrum of GRB 060218 (spectrum 6) as a function of the redshift. The eXTP detector would trigger on GRB 060218 up to redshift $z = 0.01$.

Table A.1. *Swift*-BAT+XRT (0.3−150 keV) spectral fit data results of the GRB 100316D dataset.

#	Δt	γ	$E_{\rm cutoff}$	Norm CPO	Flux BAT (10^{-9})	Flux XRT (10^{-9})	χ^2/d.o.f.
	(s)		(keV)	Photons keV^{-1} cm^{-2} s^{-1}	(erg/cm^2/s)	(erg/cm^2/s)	
1	297	$1.75^{+0.84}_{-0.68}$	$45.3^{+48.5}_{-21.2}$	$1.31^{+2.77}_{-1.30}$	4.13	–	63.7/55
2	200	$1.32^{+0.03}_{-0.03}$	$35.7^{+5.18}_{-4.35}$	$0.28^{+0.01}_{-0.01}$	3.97	2.23	856.2/814
3	394	$1.29^{+0.03}_{-0.03}$	$20.7^{+2.59}_{-2.28}$	$0.28^{+0.01}_{-0.01}$	2.07	2.04	880.6/895

Notes. For the first spectrum, we used BAT data alone.

Table A.2. *Swift*-BAT (15−150 keV) spectral fit data results of the GRB 161219B dataset.

#	Δt	γ	$E_{\rm cutoff}$	Norm CPO	Flux BAT (10^{-9})	χ^2/d.o.f. (10^{-9})
	(s)		(keV)	Photons keV^{-1} cm^{-2} s^{-1}	(erg/cm^2/s)	
1	21	$2.20^{+1.55}_{-0.85}$	–	$3.0^{+8.3}_{-2.9}$	5.1	51.6/56
2	3	$1.51^{+0.28}_{-0.31}$	$112.8^{+212.5}_{-47.9}$	$11.5^{+13.5}_{-6.6}$	170.8	79.8/77
3	4	$1.21^{+0.29}_{-0.32}$	$68.0^{+51.1}_{-22.2}$	$4.7^{+5.8}_{-2.7}$	156.7	84.9/77
4	33	$2.05^{+0.35}_{-0.32}$	–	$2.8^{+6.3}_{-2.7}$	8.4	55.2/78

Appendix B: Simulated light curves

In this section we report the simulated light curves for the three instruments we analysed and that could have led to a positive detection of an emission like that of GRB 060218. These instruments could have detected only a fraction of the total emission. The x axis covers the total time extension of the dataset we analysed.

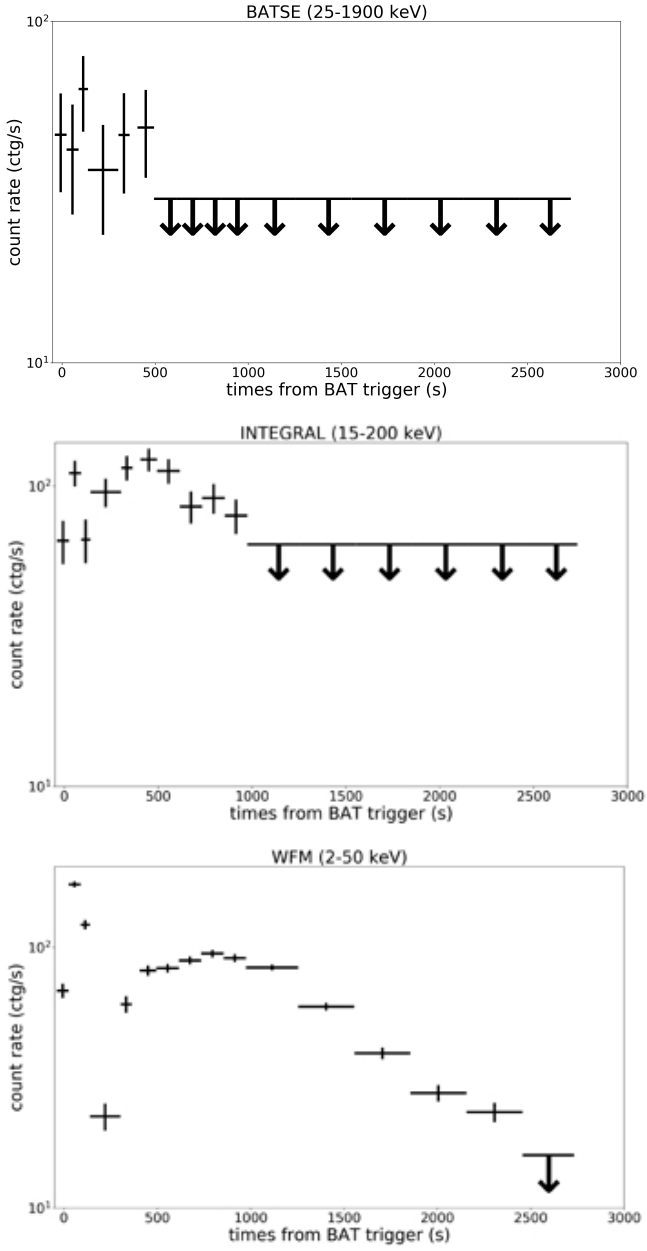

Fig. B.1. Light curve of GRB 060218 as seen by BATSE, INTEGRAL and the WFM-eXTP according to our simulations. The last intervals of our analysis would have been below the detection threshold of the instrument, and therefore no counts are expected.

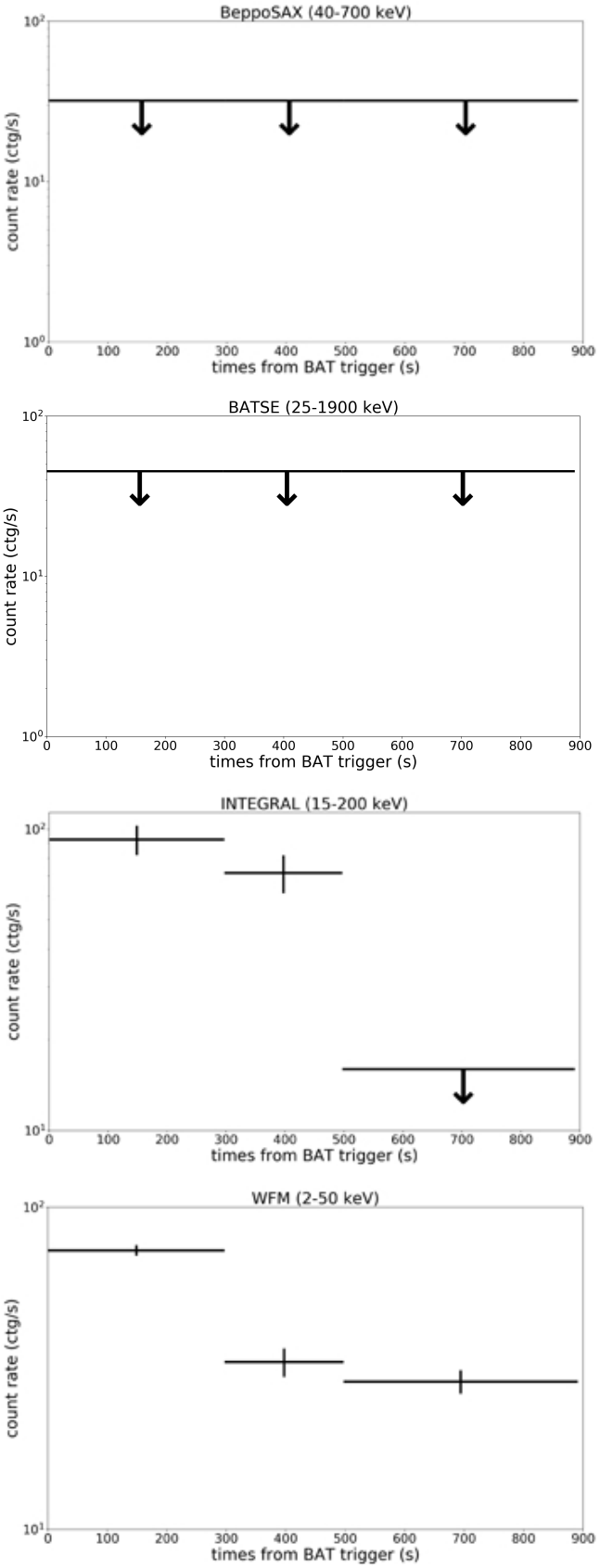

Fig. B.2. Light curve of GRB 100316D as seen by *Beppo*-SAX, BATSE, INTEGRAL, and the WFM-eXT according to our simulations.

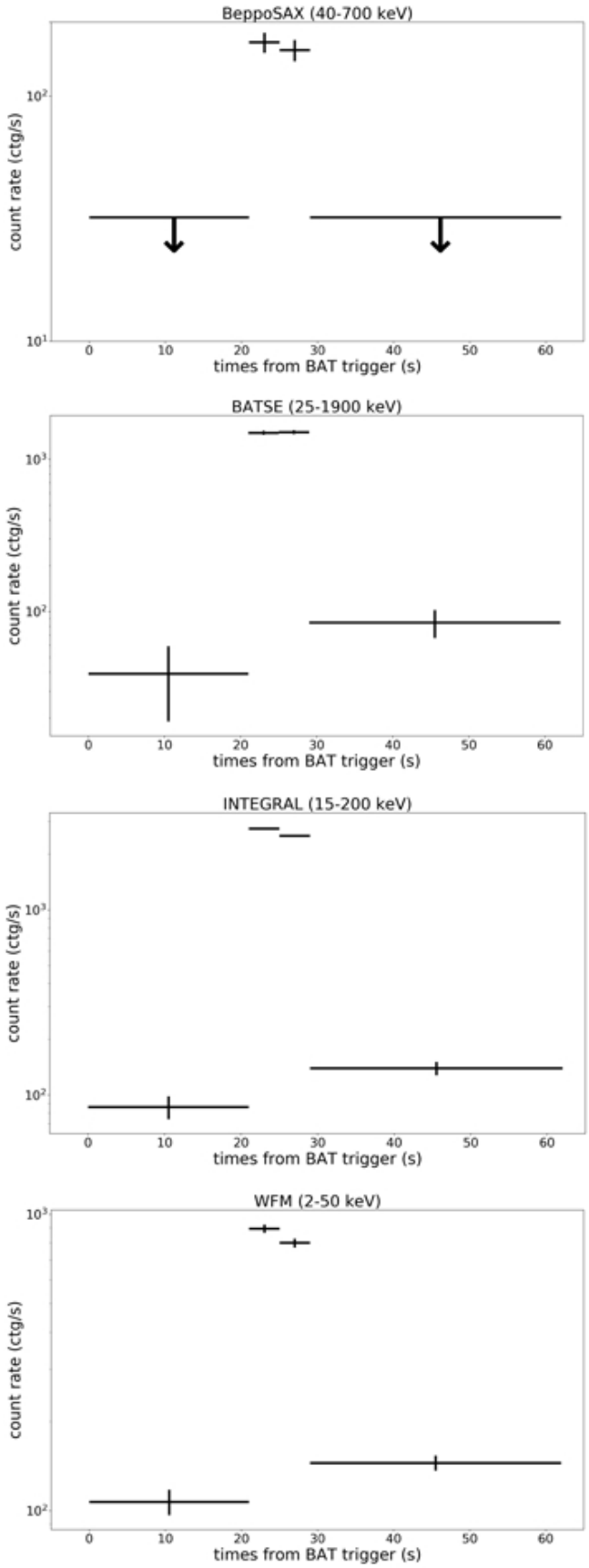

Fig. B.3. Light curve of GRB 161219B as seen by *Beppo*-SAX, BATSE, INTEGRAL, and the WFM-eXTP, according to our simulations.